

C_{60} in intense femtosecond laser pulses: plasmon excitation and multiphoton ionization

D. Bauer,¹ F. Ceccherini,^{1,2} A. Macchi,² and F. Cornolti²

¹Theoretical Quantum Electronics (TQE), Darmstadt University of Technology, Hochschulstr. 4A, D-64289 Darmstadt, Germany

²INFN, sez. A, Dipartimento di Fisica, Università di Pisa, Piazza Torricelli 2, 56100 Pisa, Italy
(May 20, 2019)

We study the interaction of strong femtosecond laser pulses with the C_{60} molecule employing time-dependent density functional theory with the ionic background treated in a jellium approximation. The laser intensities considered are below the threshold of strong fragmentation but too high for perturbative treatments such as linear response because of ionization and higher order processes. The nonlinear response of the model to excitations by pulses of frequencies up to 45 eV is presented. With the help of Kohn-Sham orbital-resolved dipole spectra the formation of collective resonances is analyzed. In femtosecond laser pulses of 800 nm wavelength ionization is found to occur multiphoton-like rather than via plasmon excitation.

PACS numbers: 36.40.-c, 33.80.Rv, 31.15.Ew

I. INTRODUCTION

Intense laser atom interaction exhibits nonlinear phenomena such as above threshold ionization (ATI), high harmonic generation (HHG), and nonsequential multiple ionization (NSI) (see [1] for recent reviews). While some of those features are accessible in terms of a sequential "single active electron" (SAE) approach others are clear manifestations of many electron effects and correlation, e.g., NSI. The full ab initio solution of the time-dependent Schrödinger equation (TDSE) for two active electrons interacting in their full dimensionality with the laser and their parent ion is already at the limit of what is possible with modern computers [2]. Treating many electron systems in laser fields thus needs further approximations. Density functional theory (DFT), extremely successful in electronic structure calculations of many-electron systems (see, e.g., [3]), has been extended to the time-dependent case (TDDFT) (see [4], and, e.g., [5] for a review). Despite the fact that TDDFT still lacks an equally solid foundation compared to that on which ground state DFT is built, it was successfully applied to metal clusters in laser pulses (see [6] for a review). Problems mainly arise when observables have to be extracted which are not obvious functionals of the Kohn-Sham orbitals or the total electron density, like in the study of NSI of atoms within TDDFT [7], or when the results are very sensitive to the choice of the approximation to the unknown exchange-correlation potential. Compared to laser atom interaction, in big molecules or clusters additional degrees of freedom are introduced: electronic degrees of freedom, including collective effects such as the formation of plasmons, vibrational degrees of freedom, or fragmentation. With laser pulses of different duration the equilibration of energy among the various channels can be probed. For C_{60} this was nicely demonstrated in Ref. [8] where the photoelectron spectra in fs laser pulses exhibited ATI peaks, a signature for direct multiphoton processes, which disappeared for longer pulses where collective effects set in. Concerning the ionization mechanism of C_{60} in fs laser pulses there is a discrepancy in the literature. While in the recent work of Tchapyguine et al. [9] from ion yield-curves vs. laser intensity direct multiphoton ionization was found to be the responsible pathway for ionization of C_{60} , in an earlier publication Hunsche et al. [10] claimed it is the excitation of a giant resonance near 20 eV. Such a resonance at 20 eV in C_{60} was first predicted theoretically by Bertsch et al. [11] and confirmed later in an experiment by Hertel et al. [12] using synchrotron radiation for single-photon ionization measurements. When compared to metal clusters where collective resonances occur at a few eV a 20 eV giant resonance is quite remarkable.

The nonlinear TDDFT treatment of C_{60} in a laser pulse is numerically rather demanding because one has to allow for ionization which implies the use of a big numerical grid in order to represent the time-dependent Kohn-Sham (KS) orbitals properly. It is thus impossible, at least with computers nowadays available, to achieve both a detailed account of the soccer ball-like structure of C_{60} and an accurate propagation of freed electron density far away from the ion and, possibly, back. Therefore we restrict ourselves to a jellium approach for the ionic background of the C_{60} . Such a jellium model was employed in [13] to study the photoabsorption of atoms inside C_{60} within linear response theory. It was found to share many of the relevant features with more demanding "first principle" calculations (like, e.g., in [11]) and experiment [12]. Jellium models were also successfully applied to metal clusters (see [14] for a review).

The paper is organized as follows. In Section II we present our TDDFT-jellium model of laser C_{60} interaction. In Section III we present results: in IIIA we characterize our model concerning the dipole response and ionization after excitation by pulses of different frequencies. The formation of collective resonances is interpreted with the help of Kohn-Sham orbital-resolved dipoles vs. time and the corresponding spectra. In IIIB we examine the ionization mechanism of our C_{60} model in 800 nm fs laser pulses. Section IV contains a brief summary and conclusion.

II. THE MODEL: STATIC PROPERTIES

The time-dependent Kohn-Sham (TDKS) equation for the orbital $\phi_i(r;t)$ reads (atomic units are used unless noted otherwise)

$$i\frac{\partial}{\partial t}\phi_i(r;t) = \left[-\frac{1}{2}\nabla^2 + V(r) + V_I(t) + V_{ee}[n_\uparrow(r;t);n_\downarrow(r;t)] \right] \phi_i(r;t) \quad (1)$$

Here, \uparrow, \downarrow indicates the spin polarization, $V(r)$ is the potential of the ions, $V_I(t)$ is the laser in dipole approximation, and $V_{ee}[n_\uparrow; n_\downarrow]$ is the effective electron-electron interaction potential which is a functional of the electron spin densities

$$n_\sigma(r;t) = \sum_{i=1}^N |\phi_i(r;t)|^2 \quad (2)$$

N is the number of orbitals occupied by Kohn-Sham (KS) particles with spin σ . The total electron density is

$$n(r;t) = \sum_{\sigma} n_\sigma(r;t) \quad (3)$$

The electron-electron potential is splitted,

$$V_{ee}[n_\uparrow; n_\downarrow] = U[n] + V_{xc}[n_\uparrow; n_\downarrow]; \quad (4)$$

where $U[n]$ is the Hartree potential

$$U[n] = \int d^3r' \frac{n(r';t)}{r-r'} \quad (5)$$

and $V_{xc}[n_\uparrow; n_\downarrow]$ is the exchange correlation (xc)-part. Although the Runge-Gross theorem [4] ensures that, in principle, the time-dependent KS scheme could yield the exact density $n(r;t)$ on which all observables depend, in practice an approximation to the exchange-correlation potential $V_{xc}[n_\uparrow; n_\downarrow]$ has to be made. We chose the Slater expression

$$V_{xc}^{\text{Slater}}(r;t) = \sum_{i=1}^N \frac{n_i(r;t)}{n(r;t)} u_{xc_i}(r;t); \quad (6)$$

where $u_{xc_i} = V_{xc}^{\text{X-LDA}}[n_\uparrow; n_\downarrow] - U[n_i] - V_{xc}^{\text{X-LDA}}[n_i; 0]$, i.e., the self-interaction is removed, and the exchange-only local density approximation (X-LDA) was employed. Taking into account also correlation effects (we used the correlation energy functional of Perdew and Wang [15]) was found to have negligible effects on the results presented in this work. Moreover, we neglect spin-polarization effects, i.e., $n_\uparrow = n_\downarrow = n/2$, $n = 2 \sum_{i=1}^{N=2} |\phi_i|^2$ where N is the number of electrons. In the actual implementation less than $N=2$ KS orbitals need to be propagated because orbitals belonging to the same subshell and having the same value j_m are still degenerated when the laser (treated in dipole approximation) is on.

The dipole approximation is excellent for the laser frequencies under consideration. One might object that the interior of the C_{60} could be screened, i.e., the laser pulse might not be able to penetrate the overdense electron cloud. Indeed, in [10] the authors came to the conclusion that the laser cannot penetrate the C_{60} . Their arguments were based on the Debye length in a plasma of electron temperature 700 K. However, whether a laser pulse of wavelength λ_i and frequency ω_i is able or not able to penetrate a plasma layer of thickness L is governed by the dimensionless parameter $\eta = (\omega_p/\omega_i)^2 = \eta_i$ [16] and not by the Debye length. Since $\eta < 1$ for all our parameters we will consider in this paper the C_{60} is not a Faraday cage, and the dipole approximation is safe.

In our numerical code, the KS orbitals are expanded in spherical harmonics $Y_l^m(\theta; \phi)$. If the ground state has a closed shell structure the effective KS potential is spherical. Hence l and m are "good" quantum numbers for

the ground state configuration. In a linearly polarized laser field (in dipole approximation) the quantum numbers m remain good, i.e., there is no m -coupling through the laser because the azimuthal symmetry is retained. $V_I(t)$ introduces an $\ell=1$ -coupling only. However, orbitals with different j behave differently in the laser field. The radial KS wave functions are discretized in position space. Each time step, the effective potential has to be calculated which makes a TDKS solver significantly more time-consuming than an ordinary TDSE code running a corresponding SAE problem. The effective potential V_{ee} was expanded up to the dipole. Consequently, both the laser and V_{ee} lead to an $\ell=1$ -coupling only. We are confident that neglecting higher order multipoles of V_{ee} does not affect the validity of our conclusions [17]. The actual propagation is performed in velocity gauge using an algorithm similar to the one for the TDSE described by Muller in Ref. [18]. Probability density reaching the radial boundary of the numerical grid at 100 a.u. was removed by an imaginary potential. The eventually decreasing norm then can be interpreted as one minus the ionization probability of that orbital.

The laser is polarized in z -direction so that in velocity gauge we have

$$V_I(t) = -iA(t)\frac{\partial}{\partial z} \quad (7)$$

where $A(t)$ is the vector potential and the A^2 -term has been transformed away (see, e.g., [19]). This potential leads to the above mentioned $\ell=1$ coupling.

The ionic background is treated in a jellium approximation, i.e., the ions are thought of being smeared out over a spherical shell with outer and inner radius R_o and R_i , respectively. The ionic charge density is constant for $R_o > r > R_i$ and zero otherwise. The radii R_o, R_i are centered around the known radius of the C_{60} -fullerene, $(R_o + R_i)/2 = R = 6.7$ a.u. In real C_{60} there are 60 π -electrons and 180 σ -electrons. Therefore the charge of the jellium background should be 240 a.u. However, 240 KS particles do not yield a self-consistent closed shell-structure for the ground state of our model. Since partially filled shells would spoil the spherical symmetry of the ground state we take 250 electrons instead (see also [13]) which leads to a self-consistent closed shell ground state of the jellium model. Thus, introducing

$$r_s^3 = \frac{N}{R_o^3 - R_i^3}; \quad N = 250; \quad (8)$$

and allowing for an additional potential depth parameter v_0 we arrive at an ionic potential

$$V(r) = \begin{cases} \frac{r_s^3}{3} (R_o^2 - R_i^2) = 2 & \text{for } r > R_o; \\ \frac{r_s^3}{3} (R_o^2 - R_i^2) + \frac{r^2 - R_i^2}{2} + \frac{R_i^3}{3} = r & \text{for } R_i < r < R_o; \\ \frac{r_s^3}{3} (R_o^3 - R_i^3) = r & \text{for } r < R_i; \end{cases} \quad v_0$$

The parameters R_o, R_i , and v_0 can be varied in order to obtain a jellium- C_{60} ground state which shares the relevant features with first-principle calculations of "real" C_{60} . We used $R_o = 8.1, R_i = 5.3$, and $v_0 = 0.78$. Some of the ground state properties of the model are shown in Fig. 1. Because of the centrifugal barrier $\ell(\ell+1)=2r^2$ the total potential is ℓ -dependent, and states with high ℓ are pushed outwards. The energy levels are $2(2\ell+1)$ -degenerated. The 250 KS particles can be subdivided in 200 $n=1$ -states (the π -electrons) occupying ℓ -values from 0 up to 9, and 50 $n=2$ -states (the σ -electrons). The orbital densities are also shown. Each σ -electron wavefunction has a node near the jellium-shell radius R . The values of the single KS particle orbital eigenenergies are given in Table I. The highest occupied state is the state with $\ell=4$. From Koopman's theorem we therefore expect an ionization energy of $I_p^+ = 0.274$. Calculating the ionization energy by subtracting the total energy of C_{60}^+ from that for neutral C_{60} we obtain (on our numerical grid with a grid spacing $\Delta r = 0.3$) $I_p^+ = 0.279$ (7.59 eV) which agrees reasonably well with the former value and experiment (7.6 eV, [20]). In any case we expect for 800 nm laser light few photons being necessary for removing the outer electron. However, collective effects might occur so that more photons are required. In fact, there is an unresolved discrepancy in the literature about whether ionization of C_{60} in the fs-regime works multiphoton-like [9] or through the excitation of a 20 eV giant resonance [10]. The results from our model concerning this question will be presented in Section IIIB.

In Table I we also enumerated the KS orbitals for the sake of easy reference later on. Since in each ℓ -subshell there are $2\ell+1$ different j -values we need 70 KS orbitals to describe our jellium-model interacting with the laser field. In each ℓ -subshell the KS orbitals are labeled from $m=0$ up to $j=\ell$. Thus, e.g., orbital no. 0 refers to the two electrons of opposite spin which, in the ground state configuration, populate the $n=1, \ell=m=0$ state whereas orbital no. 69 is initially a pure $n=2, \ell=j=4$ state, populated by four electrons with different spin and/or sign of m .

III. RESULTS

In this Section we present results obtained with our TDDFT code which propagates the KS orbitals in time, starting from the ground state discussed in the foregoing Section. In the first Subsection we study the dipole spectra and ionization of our model after the interaction with light pulses of different frequencies. In the second Subsection we focus on the slope of the ion yield vs. laser intensity which gives the photon order of the ionization mechanism, i.e., it allows to distinguish between direct multiphoton ionization or excitation of a more energetic collective mode such as the 20 eV resonance.

A. Ionization and plasmon excitation

Within linear response theory plasmon excitations are commonly inferred from the photo absorption cross section, i.e., the imaginary part of the polarizability. Here we follow the different route of nonlinear TDDFT which allows us to distinguish between ionization, plasmon excitation, or both together, and also accounts for higher order processes beyond single particle hole excitations.

We calculated the interaction of our jellium model with ten cycle \sin^2 -shaped (with respect to the electric field) laser pulses in the frequency range from 6.8 up to 47.6 eV. The peak intensity was adjusted in such a way that intensity times pulse duration (energy per unit area) was held constant, i.e., in atomic units $\hat{A}^2 \omega_i = 1.8375 \cdot 10^5$ where ω_i is the incident laser frequency and \hat{A} is the vector potential amplitude. With such laser intensities the probability to remove the first electron remained below 10% for all frequencies. After the laser pulse was over we continued the propagation of all KS orbitals to allow for delayed ionization and free oscillations. The total simulation time corresponded to $t_{\text{end}} = 11.5$ fs so that a real C_{60} which has been ionized at most to C_{60}^+ has no time for fragmentation. From the Fourier-transformed dipole $d(t) = \int d^3r \rho(r) \mathbf{r}$ it is possible to calculate at which frequencies our C_{60} model would emit radiation. In particular, by Fourier-transforming over a time interval after the laser pulse is over only the eigenmodes remain. The result is presented in Fig. 2. The contour plot shows the logarithmically scaled dipole strength vs. incident frequency ω_i and emitted frequency ω_e . Left to the contour plot the number of removed electrons

$$N_{\text{rem}} = 250 \int_{\text{Grid}} d^3r n(\mathbf{r}; t_{\text{end}})$$

is plotted as a function of the incident frequency ω_i . In all cases delayed ionization was negligible compared to the electron density which was freed owing to the laser pulse.

All strongly excited plasmons lie near the diagonal $\omega_i = \omega_e$ where the excitation was resonant. However, at $\omega_i = \omega_e = 20.5$ eV relatively few plasmons were excited. It is exactly there where the ionization yield has a local maximum (dashed line). Instead, the local minima in ionization at 17 and 24 eV coincide with two strong resonances near the same values for ω_e . This is not surprising: while in the former case laser energy is used to set electron density free, in the latter case it is used to excite plasmons keeping the electron density trapped. From the photo absorption cross section in linear response theory one can hardly distinguish between both cases. For $\omega_i = 30$ eV one observes both, strong ionization and efficient plasmon excitation. For even higher ω_i ionization drops and the jellium system does not provide any collective modes > 40 eV.

The linear response result for the photo absorption cross section presented in [13] for a similar jellium model shows two pronounced peaks (although at somewhat lower energies) which resemble our peaks at $\omega_e = 17$ and 24 eV. Such peaks are commonly interpreted as surface plasmons, so-called Mie-resonances [21]. Such Mie-plasmons have frequencies

$$\omega_{\text{Mie}, \lambda} = \frac{\omega_p}{\sqrt{2\lambda + 1}}$$

where ω_p is the bulk plasma frequency and λ is the index of a multipole expansion. For a dipolar Mie-plasmon we simply have $\omega_{\text{Mie}} = \omega_p / \sqrt{3}$. For our model we expect the Mie-resonance at 21.9 eV. Usually the peaks are found to be red-shifted which is attributed to the spill-out effect when the electron density oscillates beyond the jellium background into the vacuum. Therefore one might think about the peak at 17 eV in terms of a surface plasmon. We checked this by looking at movies of the oscillating total electron density (minus the ground state electron density). Not surprisingly, we observed at a certain time instant excess electron density at $z = +R_a$, missing electron density at $z = +R_i$, excess at $z = -R_i$ and another lack of density at $z = -R_a$ while one half period later it is the other way round. However, this dipole-like motion is qualitatively the same for all other frequencies as well. "Real space movies" are therefore not very suited for an understanding of the positions of those plasmon peaks.

On the other hand, the position of all the plasmon peaks in Fig. 2 can be understood in terms of transitions between the KS energy levels of Table I. To illustrate this we present KS orbital-resolved dipoles (KSORD) vs. time and the corresponding spectrum (KSORD-spectrum). For $I_i = 0.9 \text{ a.u.}$ (the 24 eV-peak) the result is given in Fig. 3. From the KSORD we infer how each KS orbital, populated by either two particles ($m = 0$) or four particles ($m > 0$), oscillates after the laser pulse is over. The different ℓ -shells can be easily distinguished. The amplitude of the total dipole is relatively small because the individual KS orbital dipoles in part interfere destructively. In general the ℓ -electrons (orbital numbers 0{54}) tend to oscillate 180° out of phase with respect to the ℓ -electrons (55{69}) of the same (initial) ℓ . The spectrum of the KSORD is presented at the right-hand-side of Fig. 3. The low frequency lines in the range 0{5 eV stem from transitions of the type $\ell' \rightarrow \ell - 1$ with the n -quantum number fixed. Instead, the plasmons positioned along a parabola-like structure around 20 eV originate from transitions of the type $(n = 1) \ell' \rightarrow (n = 2)(\ell + 1)$ or $(n = 2) \ell' \rightarrow (n = 1)(\ell - 1)$ (right branches) and $(n = 1) \ell' \rightarrow (n = 2)(\ell - 1)$ or $(n = 2) \ell' \rightarrow (n = 1)(\ell + 1)$ (left branches). The ℓ -electrons also make transitions between 5 and 15 eV. Those peaks can be stronger for lower I_i and are caused by transitions $(n = 2) \ell' \rightarrow (n = 3)(\ell - 1)$. Another striking feature for all $\ell = j_n$ orbitals (i.e., orbitals number 0, 2, 5, 9, 14, 20, 27, 35, 44, 54, 55, 57, 60, 64, 69) is their common peak near 28 eV. This energy corresponds to a transition of the type $(n = 1) \ell' \rightarrow (n = 3)$. The reason why the $\ell = j_n$ orbitals preferably radiate at that frequency is that $\ell' \rightarrow \ell - 1$ transitions are not possible for them. Indeed, the left branch of the parabola-like structure for the ℓ -electrons (related to transitions where the ℓ -quantum number decreases by one) shows gaps for the $\ell = j_n$ orbitals whereas for the ℓ -electrons it is the right branch where the corresponding lines are missing. The spectrum of the total dipole is shown above the contour plot. Although individual KS orbitals strongly oscillate with frequencies between 21 and 23 eV only the line at 24.5 eV survives due to destructive interference of the former and constructive interference of the latter. In fact, in the KSORD-spectrum one sees that all KS orbitals have a relatively strong component of the 24.5 eV mode. This is nothing else than the manifestation of a giant resonance in terms of single KS particle transitions. It occurs at frequencies which correspond to single KS particle transitions of type $n \ell' \rightarrow (n - 1)(\ell - 1)$ involving ℓ -orbitals with highest occupied ℓ in the ground state configuration. Those orbitals have the highest degree of degeneracy which is favorable for collective behavior. Since the density of high- ℓ states is pushed outwards due to the centrifugal barrier it makes indeed sense to call those collective excitations surface (or Mie) plasmons. Note that the fact that in our KSORD spectrum also (initially) low- ℓ orbitals emit radiation corresponding to higher- ℓ transitions implies higher order processes beyond single particle hole excitations.

As an example for a higher incident frequency ($I_i = 1.1$) we present the KSORD in Fig. 4. All orbitals oscillate with the same frequencies around 30 eV (note the two lighter vertical stripes at the same position for nearly all the orbitals). This is a clear indication for a nonlinear process because more than a single transition from the ground state configuration to an excited state is required to meet those particular frequencies at 31.9 eV and 29.5 eV. Those energies correspond to the $(n = 3) \ell' \rightarrow (n = 1)(\ell + 1)$ transition for $\ell = 0$ and $\ell = 2$, respectively. The amplitude of the total dipole is higher than those of the individual KS orbital dipoles, indicating that the 30 eV emission is due to constructive interference of many KS orbital oscillations while, again, the low frequency modes (e.g., the one of the $\ell = 7$ -orbital at 4.6 eV) interfere away. One might argue that this is the formation of a bulk plasmon although the bulk in our model is only a spherical shell of thickness 2.8 atomic units. Assuming a homogenous electron density over the shell one finds a plasma frequency $\omega_p = 38 \text{ eV}$. A red-shift of 10{20% is usually attributed to spill-out effects and the non-uniform electron density.

B. C_{60}^+ yield vs. laser intensity for $\lambda = 800 \text{ nm}$

After studying the plasmon response at relatively high energies we now turn to the interaction of C_{60} with laser light of 800 nm wavelength. We simulated the interaction of our C_{60} jellium model with a ten cycle 800 nm \sin^2 -shaped laser pulses (corresponding to 26 fs pulse duration). In Fig. 5 the removed electron density N_{rem} after the pulse vs. the peak intensity of the pulse is presented. In the regime where $N_{\text{rem}} \ll 1$ this is equivalent to the single ionization probability. In the case of perturbative off-resonant multiphoton ionization of atoms it is well-known (see, e.g., [19]) that the ionization probability is I^n where n is the number of photons needed to reach the continuum from the initial state. From Section II we know that in our jellium model the first ionization potential is $I_p^+ = 0.279$, and thus we expect $n = 5$ photons necessary for ionization if C_{60} behaves multiphoton-like. As is evident from Fig. 5 this is the case, in agreement with an experiment performed using a Ti:Sapphire laser ($\lambda = 800 \text{ nm}$, 30 to 120 fs pulse duration) [9]. There, from the C_{60}^{2+} yield-slope, also the second electron was found to behave multiphoton-like with $n = 8$. Those findings are in contrast with earlier experimental results in [10] (same wavelength and pulse durations) where excitation of the 20 eV Mie-resonance, corresponding to $n = 13$ photons, was concluded to be the dominant ionization mechanism. The $n = 13$ slope is depicted in Fig. 5 in the upper left corner and is much too steep to fit with our numerical result. This appears reasonable because the incident laser frequency 1.6 eV lies energetically far below

the Mie-resonance so that an efficient excitation of the latter is unlikely. The experimental fragmentation onset and the C_{60} saturation intensity as observed in [9] is also indicated in Fig. 5.

In Fig. 6 we present dipoles and the corresponding spectra for two particular laser intensities. For the higher intensity [plots (c) and (d)] the electron density continues oscillating quite strongly after the pulse but with little effect on ionization. In the spectra (b) and (d) the black curve was calculated from Fourier-transforming the dipole with respect to the entire time interval shown in the plots above. Therefore lines corresponding to the laser harmonics can be observed in those spectra. Fourier-transforming only over the time after the pulse leads to the gray curves. In the low intensity case (b) the dominant line is around 3 eV, corresponding to the transition of the outermost π -electron from $\ell = 4$ to $\ell = 5$. This transition is nearly resonant with two laser photons. In the high intensity case the electron density continues oscillating with the laser frequency even after the pulse. The next more energetic peaks are, again, the $\ell = 4 \rightarrow 5$ transition near 3 eV followed by the $\ell = 9 \rightarrow 10$ transition of a π -electron at 5.5 eV. The next line corresponds to the ionization energy 7.5 eV. For both intensities excitations around 20 eV are several orders of magnitude weaker and can therefore not play any role in the ionization process of our C_{60} model at that laser wavelength.

IV. CONCLUSION

In this paper we presented a nonlinear time-dependent density functional theory (TDDFT)-treatment of a C_{60} jellium model in intense laser pulses. The Kohn-Sham (KS) orbitals were expanded in spherical harmonics and discretized in radial direction on a sufficiently big numerical grid on which they were propagated in time. By this method all bound states and the continuum can be properly represented, allowing for an accurate description of ionization and higher order transitions, not included in linear response theory (sometimes also called TDDFT).

For short exciting pulses with frequencies between 7 and 48 eV we studied both ionization and the power spectra, calculated from the nonlinear dipole response after the pulse had passed by. We observed that when the incident frequency matched with two resonant peaks of the dipole spectrum at 17 and 24 eV, respectively, ionization dropped. Instead, an incident frequency in between (≈ 20.5 eV) led to a maximum ion yield. Another maximum was found at frequencies around 31 eV where strong ionization and plasmon excitation occur together. For even higher incident photon energies > 37 eV ionization decreased because energy transfer to the C_{60} became inefficient.

We characterized in detail the Kohn-Sham orbital resolved dipole (KSORD) response. The corresponding spectra can be understood in terms of transitions between the unperturbed KS orbital energy levels connected to the ground state. In the KSORD spectra the formation of, e.g., the 24 eV Mie-resonance (i.e., surface plasmon) appeared as the destructive interference of single KS orbital oscillations with low frequency, and constructive interference of the higher frequency oscillation. Those Mie-plasmons form at frequencies of the KSORD spectrum which stem from single KS particle transitions of type $n \rightarrow (n+1)$ involving the ℓ and $\ell+1$ orbitals with highest occupied ℓ (in the ground state configuration). This is because these ground state orbitals have the highest degree of degeneracy which supports collective behavior.

For 800 nm fs laser pulses we observed direct multiphoton ionization rather than ionization via excitation of a Mie-resonance. This result agrees with recent experimental findings in [9]. Although it disagrees with earlier results in [10] we are quite confident that our model also works well in this respect because the multiphoton character for optical (or near optical) frequencies is well-known for metal clusters (see, e.g., [6], and references therein), and it is hard to believe that it should be different for C_{60} where the collective resonances are even more energetic.

The TDDFT jellium model offers one of the very few feasible approaches for theoretical investigations concerning the interaction of intense laser light with complex systems where many electron-effects, bound-free transitions, and rescattering might be important. Preliminary results for "above threshold ionization" (ATI) of C_{60} (as in the experiment [8]) were also obtained within this model [22]. Simulating ATI is always much more demanding than studying the dipole response and ionization only since one has to trace the free electron motion in the continuum as well as rescattering events with very high accuracy over several laser cycles of optical frequency.

ACKNOWLEDGMENT

This work was supported by the FUMOFIL project through the INFN Parallel Computing Initiative, and by the Deutsche Forschungsgemeinschaft within the SPP "Werkzeug zur Entwicklung intensiver Laserfelder in der Materie." Illuminating discussions with D. P. Itrelli are gratefully acknowledged.

- [1] M . Protopapas, C . H . Keitel, and P . L . Knight, Rep. Progr. Phys. 60, 389 (1997); C . J . Joachain, M . Dorr, and N . J . Kylstra, Adv. At. Mol. Opt. Phys. 42, 225 (2000).
- [2] E . S . Smyth, J . S . Parker, and K . T . Taylor, Comput. Phys. Commun. 114, 1 (1998); J . S . Parker, L . R . Moore, D . D . Dundas, and K . T . Taylor, J. Phys. B: At. Mol. Opt. Phys. 33, L691 (2000).
- [3] R . M . Dreizler and E . K . U . Grosse, \Density Functional Theory: An Approach to the Quantum Many-Body Problem," (Springer, Berlin, 1990).
- [4] Erich Runge and E . K . U . Grosse, Phys. Rev. Lett. 52, 997 (1984).
- [5] Kieron Burke and E . K . U . Grosse, A Guided Tour of Time-Dependent Density Functional Theory in: \Density Functionals: Theory and Applications" ed. by Daniel Joubert, (Springer, Berlin, 1998), p. 116.
- [6] F . Calvayrac, P . G . Reinhard, E . Suraud, and C . A . Ulrich, Phys. Rep. 337, 493 (2000).
- [7] C . A . Ulrich and E . K . U . Grosse, Comm. At. Mol. Phys. 33, 211 (1997); M . Petersilka and E . K . U . Grosse, Laser Physics 9, 105 (1999); D . Bauer and F . Ceccherini, Optics Express 8, 377 (2001).
- [8] E . E . B . Campbell, K . Hansen, K . Homann, G . Kom, M . Tchapyguine, M . W ittmann, and I . V . Hertel, Phys. Rev. Lett. 84, 2128 (2000).
- [9] M . Tchapyguine, K . Homann, O . D uhr, H . Hohmann, G . Kom, H . Rottke, M . W ittmann, I . V . Hertel, and E . E . B . Campbell, J. Chem. Phys. 112, 2781 (2000).
- [10] S . Hunsche, T . Starczewski, A . H uillier, A . Persson, C . G . Wahlstrom, B . van Linden van den Heuvell, and S . Svanberg, Phys. Rev. Lett. 77, 1966 (1996).
- [11] George F . Bertsch, Aurel Bulgac, David Tomaneck, and Yang Wang, Phys. Rev. Lett. 67, 2690 (1991).
- [12] I . V . Hertel, H . Steger, J . de Vries, B . Weisser, C . Menzel, B . Kamke, and W . Kamke, Phys. Rev. Lett. 68, 784 (1992).
- [13] M . J . Puska, and R . M . Nieminen, Phys. Rev. A 47, 1181 (1993).
- [14] M . Brack, Rev. Mod. Phys. 65, 677 (1993).
- [15] John P . Perdew and Yue Wang, Phys. Rev. B 45, 13244 (1992).
- [16] V . A . V shirkov, N . M . Naumova, F . Pegoraro, and S . V . Bulanov, Phys. Plasmas 5, 2727 (1998).
- [17] We could reproduce all results presented in this paper even stopping the multipole expansion of the effective potential already after the monopole. Only slight quantitative changes were the result but no qualitative differences were observed.
- [18] H . G . Muller, Laser Physics 9, 138 (1999).
- [19] F . H . M . Faisal, Theory of Multiphoton Processes (Plenum Press, New York, 1987).
- [20] G . Seifert, K . Vietze, and R . Schmidt, J. Phys. B: At. Mol. Opt. Phys. 29, 5183 (1996), and references therein.
- [21] G . Mie, Ann. Phys. (Leipzig) 25, 377 (1908).
- [22] D . Bauer et al., unpublished.

TABLE I. The ground state single KS particle orbital energies as obtained on our numerical grid used for propagation with grid spacing $r = 0.3$. The σ -electrons occupy l -values up to 9, the π -electrons up to 4. Orbital energies of unoccupied levels are written italic. The orbitals are enumerated for the sake of easy reference. For each l -shell $l + 1$ KS orbitals to account for all the possible m_l (numbered from lowest to highest) are needed.

FIG. 1.

Ground state properties of the jellium C_{60} -model. (a) The total potential $V(r) + U[n(r)] + V_{xc}[n(r)]$ depends on the angular quantum number l (through the centrifugal barrier). For $n = 1$ (σ -electrons) orbitals from $l = 0$ up to $l = 9$ are occupied in the ground state situation, for $n = 2$ (π -electrons) orbitals from $l = 0$ to $l = 4$ are occupied. The potential for the empty $l = 10$ orbitals is drawn dashed. The radial shape of the total ground state density $n(r)$ is also plotted. (b) The single KS particle energy levels corresponding to the potentials in (a). σ -states are drawn solid while π -states are plotted dashed. The degeneracy is $2(l + 1)$. (c) The orbital densities $n_l(r)$. The sum of those is $n(r) = 4$.

FIG. 2.

Right-hand-side: contour plot of the Fourier-transformed dipole $d(t)$ after ten cycle pulses of frequency ω_i . The dipole strength vs. incident frequency ω_i and emitted frequency ω_e is logarithmically scaled (cf. color bar ranging from 10^{-30} to 10^{-7} , in arbitrary units). Left-hand-side: number of removed electrons. The horizontal solid (dashed) lines indicate frequencies ω_i where ionization was relatively low (high) and plasmon excitation was efficient (inefficient).

FIG. 3.

KS orbital resolved dipoles (KSORD, left) and the corresponding spectrum (right) after a laser pulse with frequency $\omega_i = 0.9$. The KS orbitals are enumerated according Table I. The total dipole and the corresponding spectrum (linearly scaled) are given also. See text for a detailed discussion.

FIG. 4.

Same as in Fig. 3 but for $\omega_i = 1.1$. See text for a detailed discussion.

FIG. 5.

Removal of the first electron vs. the peak intensity of a ten cycle 800 nm \sin^2 -pulse (solid curve). A multiphoton-like behavior with $n = 5$ is evident. Instead, $n = 13$ photons would be necessary to excite the 20 eV Mie-resonance. Fragmentation threshold and C_{60}^+ saturation intensity from [9] are also indicated (vertical lines).

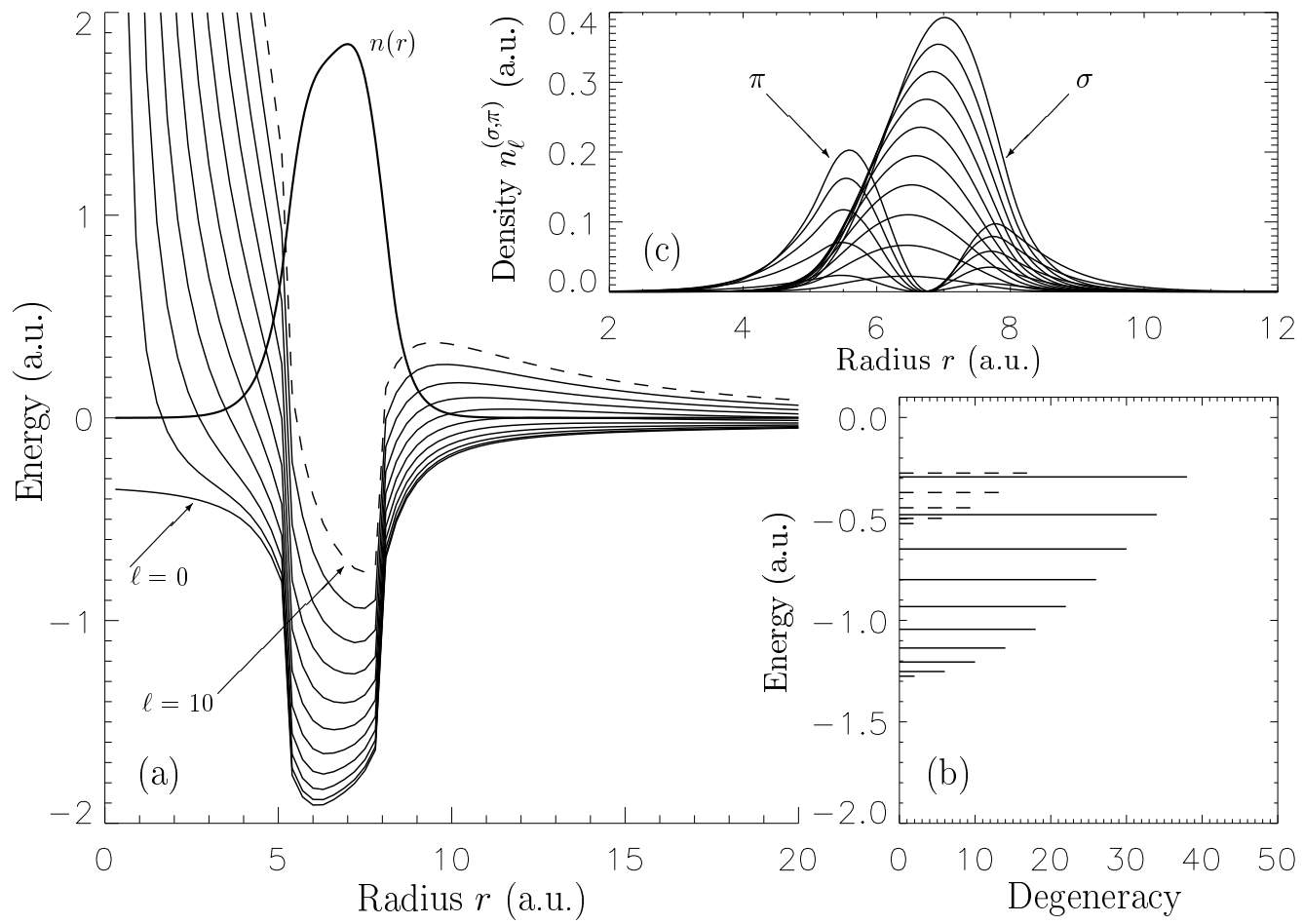
FIG. 6.

Dipole $d(t)$ [plots (a) and (c)] and its Fourier transformation [plots (b) and (d)] for a ten cycle 800 nm \sin^2 -pulse of peak intensity $I = 4.56 \cdot 10^{12} \text{ W/cm}^2$ [plots (a) and (b)] and $I = 2.85 \cdot 10^{13} \text{ W/cm}^2$ [plots (c) and (d)]. The black spectra are calculated from the entire time interval, the gray curves (multiplied by 10^4 , for better legibility) are spectra calculated from the time after the laser pulse. The former exhibit laser harmonics while in the latter single particle hole-excitations at low energies are dominant. Excitations $> 15 \text{ eV}$ are many orders of magnitude too weak for having a strong effect on ionization.

\	=	0	1	2	3	4	5	6	7	8	9	10
n = 1		-1.275	-1.252	-1.205	-1.136	-1.044	-0.932	-0.799	-0.648	-0.478	-0.293	-0.092
orb.no.		0	1,2	3{5	6{9	10{14	15{20	21{27	28{35	36{44	45{54	
n = 2		-0.523	-0.497	-0.445	-0.370	-0.274	-0.159	-0.031	-0.006	-0.002		
orb.no.		55	56,57	58{60	61{64	65{69						
n = 3		-0.080	-0.068	-0.052	-0.034	-0.021	-0.014	-0.010				

Table 1: D. Bauer et al., $\backslash C_{60}$ in intense fem to second laser pulses ..."

Fig. 1: D. Bauer et al., \C 60 in intense fem tosecond laser pulses ..."



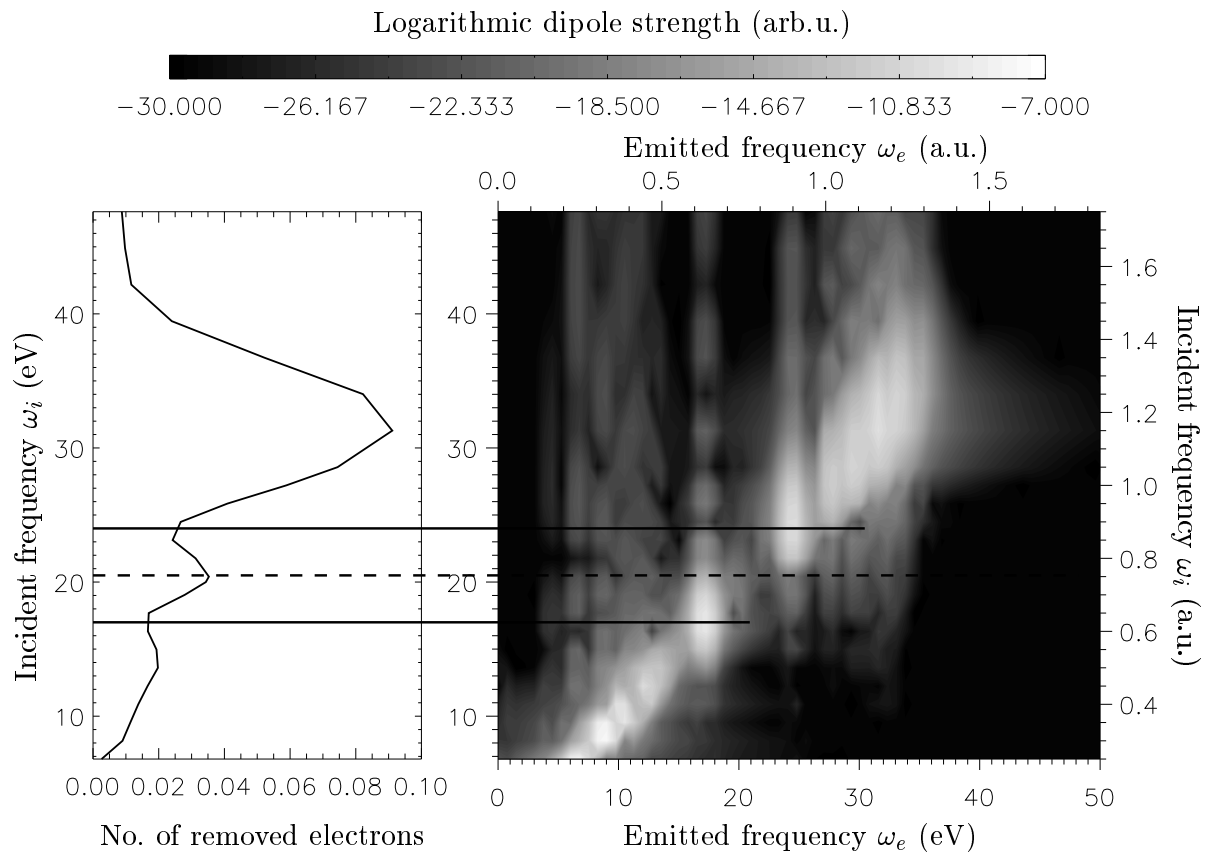


Fig. 2: D. Bauer et al., "C₆₀ in intense femtosecond laser pulses ..."

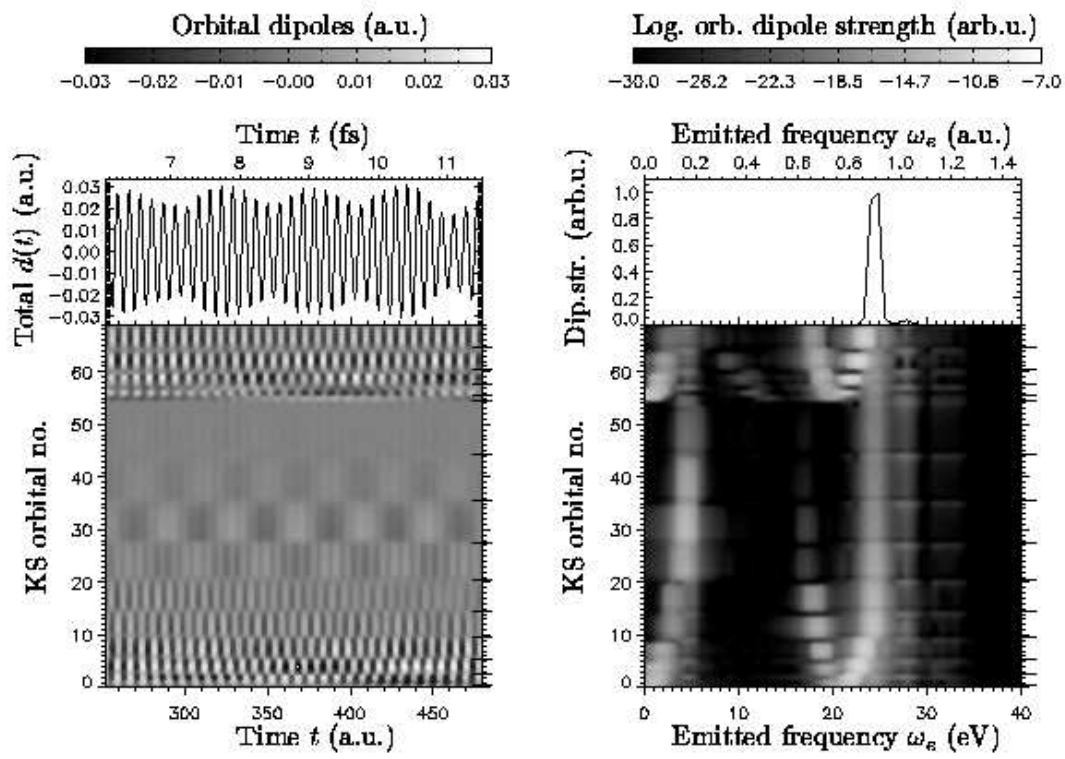


Fig. 3: D. Bauer et al., "C₆₀ in intense femtosecond laser pulses ..."

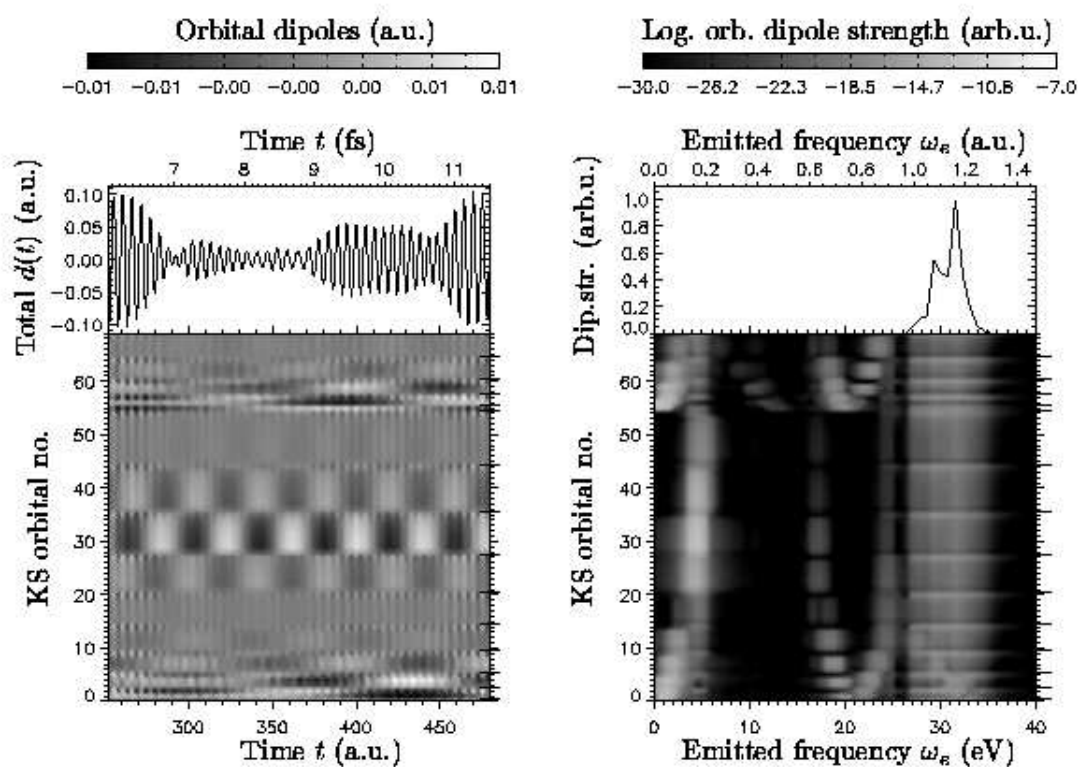


Fig. 4: D. Bauer et al., "C₆₀ in intense femtosecond laser pulses ..."

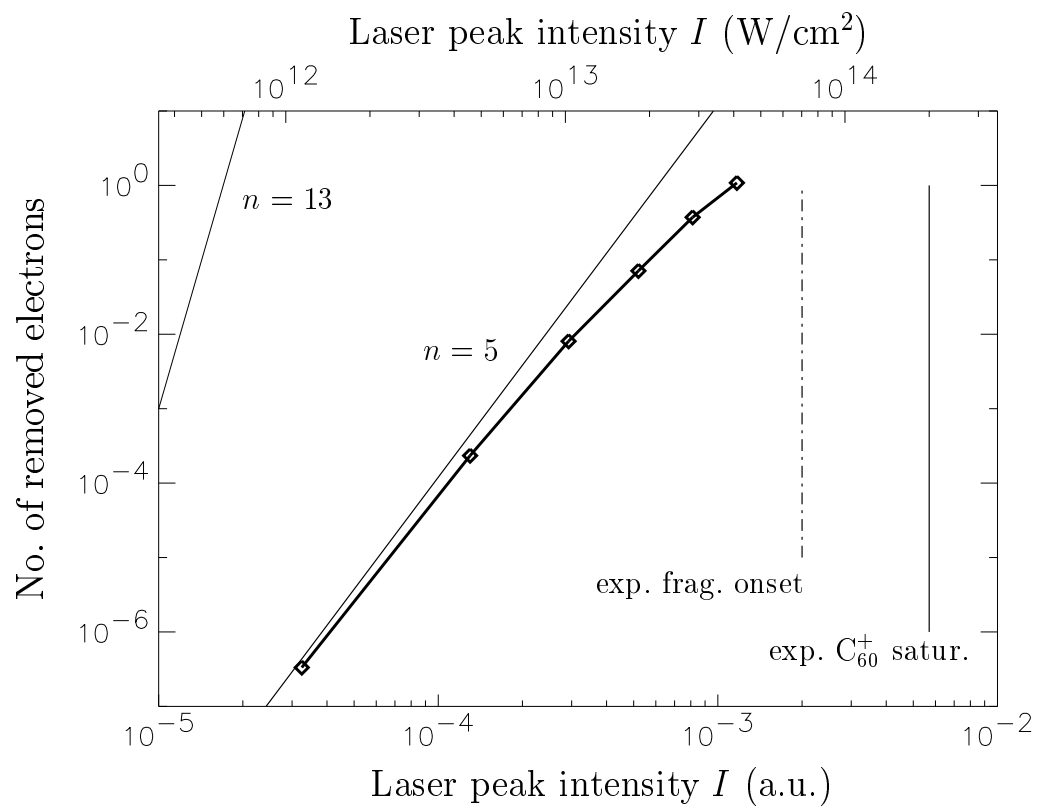


Fig. 5: D. Bauer et al., "C₆₀ in intense femtosecond laser pulses ..."

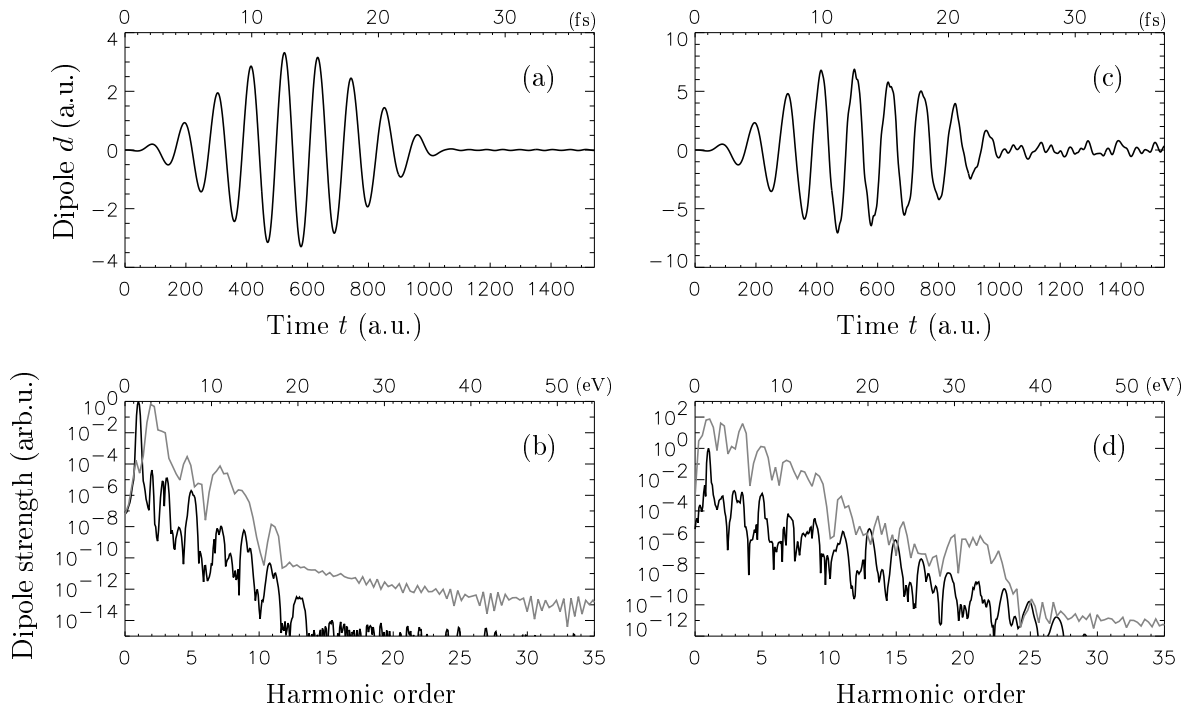


Fig. 6: D. Bauer et al., "C₆₀ in intense femtosecond laser pulses ..."